INVESTIGATING MITOCHONDRIA PENETRATING PEPTIDES WITH SOLID STATE NMR USING MODEL MEMBRANES

by

Lauren E. Marbella

BS Biochemistry, Duquesne University, 2009

Submitted to the Graduate Faculty of

the Kenneth P. Dietrich School of

Arts and Sciences in partial fulfillment

of the requirements for the degree of

Master of Science

University of Pittsburgh

2012

UNIVERSITY OF PITTSBURGH

DIETRICH SCHOOL OF ARTS AND SCIENCES

This thesis was presented

by

Lauren E. Marbella

It was defended on

June 9, 2011

and approved by

Sunil K. Saxena, Associate Professor, Department of Chemistry

Shigeru Amemiya, Associate Professor, Department of Chemistry

Committee Chair: Megan M. Spence, Assistant Professor, Department of Chemistry

INVESTIGATING MITOCHONDRIA PENETRATING PEPTIDES WITH SOLID STATE NMR USING MODEL MEMBRANES

Lauren E. Marbella, MS

University of Pittsburgh, 2012

Penetrating peptides are unique peptides that can translocate across membranes in a non-lytic fashion. A new class of penetrating peptides that can target the mitochondria with high specificity have been developed. Targeting the mitochondria is therapeutically valuable, given the organelle's role in energy production and apoptosis. The peptide we studied is sufficiently cationic and hydrophobic and is hypothesized to reach the mitochondrial matrix.[2] However, the mechanism of translocation remains unknown. In our work, we use solid state NMR to gain insight into the mechanism of translocation of this mitochondria-penetrating peptide. We use static ^{31}P NMR the membrane morphology and peptide-induced structure changes. The paramagnetic relaxation effect examined through ^{13}C MAS NMR[3] was used for insertion depth determination and to distinguish bilayer sidedness. We found that the peptide does not disrupt the lamellarity. Also, at low peptide concentrations the peptide binds to the outer leaflet and at high concentrations crosses the hydrophobic bilayer core and is distributed in both leaflets. Our findings support the electroporation model of translocation, but we did not observe complete translocation of the peptide. We examine the energy associated with crossing the inner mitochondrial membrane to determine the feasibility of the peptide reaching the mitochondrial matrix.

TABLE OF CONTENTS

1.0 INTRODUCTION 1

2.0 MATERIALS AND METHODS 16

Lipids and Peptides 16

Large Unilamellar Vesicles 16

LUVs Exhibiting a Transmembrane Potential 17

NMR Spectroscopy 19

3.0 RESULTS AND DISCUSSION 21

Membrane Morphology in the Presence of Peptide 21

Location of Peptide in the Bilayer 24

Free Energy Change of Peptide Translocation 34

4.0 CONCLUSIONS AND FUTURE WORK 43

BIBLIOGRAPHY 49

LIST OF TABLES

Table 1. Lipid composition of the inner mitochondrial membrane and our models.....8

Table 2. The expected NMR results associated with each mechanism of translocation.. 11

LIST OF FIGURES

Figure 1. Proposed mechanisms used by penetrating peptides to cross membranes 3

Figure 2. Membrane barriers encountered by mitochondria-penetrating peptides 5

Figure 3. Chemical structures of lipids 8

Figure 4. The ^{31}P chemical shift anisotropy of unoriented static phospholipids 10

Figure 5. Paramagnetic relaxation effect of Mn^{2+} on peptides in lipid bilayers 15

Figure 6. The peptide does dramatically alter the structure of the membrane. 23

Figure 7. Manganese ions do not cross the bilayer and form stable one side bound samples. 25

Figure 8. The intensity of the Mn^{2+} bound sample (S) double normalized with respect to the unbound sample (S_0) and the maximum lipid peak $(S/S_0)_{max}$ 28

Figure 9. ^{13}C MAS NMR spectra illustrating the attenuation due to the PRE effect at low (P:L = 1:40) and high (P:L = 1:10) peptide concentrations. 29

Figure 10. High peptide concentration leads to distribution in both leaflets. 30

Figure 11. At both high and low peptide concentrations, the MPP is bound near C2 of the lipid acyl chain. 32

Figure 12. The energy profile associated with inserting the MPP into a plasma membrane (black) and the inner mitochondrial membrane (red) 35

Figure 13. Cristae-like invaginations that are formed in GUVs with the local addition of HCl .. 41

Figure 14. Image of the hydrogen bonding between the positively charged arginine side chain and the phospholipid headgroups..... 45

Figure 15. The +3 peptide scaffolds and the quantitation of mitochondrial localization 48

1.0 INTRODUCTION

One of the main problems of therapeutic efficiency is the inability of drugs to cross cellular membranes.[1] Therefore, a significant effort has been made to develop a method to allow drugs to cross lipid bilayers without lysing the cell.[1] Cell-penetrating peptides (CPPs) are peptides that can cross membranes in a non-lytic fashion and carry attached cargo inside the cell.[2] Once inside, the therapeutic cargo is cleaved from the peptide and can reach its appropriate target. These short protein transduction domains (<30 amino acids) typically consist of a combination of hydrophobic residues and basic, charged residues such as arginine and lysine.[2] Because of the efficient cellular uptake and low toxicity associated with these peptides, they are the ideal candidate to deliver therapeutics and are beginning to be applied in the medical field.[1] However, some weaknesses are still present, in particular, the lack of specificity towards the intended target.[1]

Several organelles within the cell are useful targets. From protein folding, to processing genetic information, to programmed cell death, each organelle plays a specific role. In order to gain access to specific organelles, it is essential to identify the properties that make an efficient penetrating peptide to tailor its selectivity towards different locations.[1] To accomplish this, it would be helpful to elucidate the mechanism of translocation, which remains largely unknown.[3-4] A variety of mechanisms have been proposed and are generally divided into two categories: endocytosis or direct translocation (Figure 1).[5] Endocytosis routes include macropinocytosis and

clathrin- and caveolin-independent endocytosis.[6] Endocytosis is an energy-dependent mechanism in which the peptide in the extracellular environment is encapsulated into a lipid vesicle and internalized after resealing the plasma membrane.

However, due to the potential dependence and preservation of bilayer, penetrating peptides are believed to proceed by direct translocation. The possible mechanisms of direct translocation include electroporation,[7-9] inverse micelles,[10-12] and guanidinium-phosphate mediated translocation.[13] In the first model,[11] inverse micelles transiently form in the bilayer to trap the peptide from the extracellular environment and release it into the cytosol. In the second model,[13] a guanidinium-phosphate complexation neutralizes the cationic residues of the peptide and allows the peptides to cross the hydrophobic core of the bilayer without a high free-energy penalty. In the electroporation model,[7] at low peptide concentrations the peptide binds to the outer leaflet of the bilayer where the cationic residues can interact with the phosphate headgroups. If the bilayer is anionic, the accumulation of positively charged residues attracts negatively charged lipids, which induces an electric field until a threshold is reached where transient pores are formed.[8] Therefore, at high peptide concentration, electroporation permeability allows the peptide to cross to the inner leaflet where it can be released into the cytosol. Due to the diversity of orangellar membranes, it is plausible that the mechanism varies for each individual target.

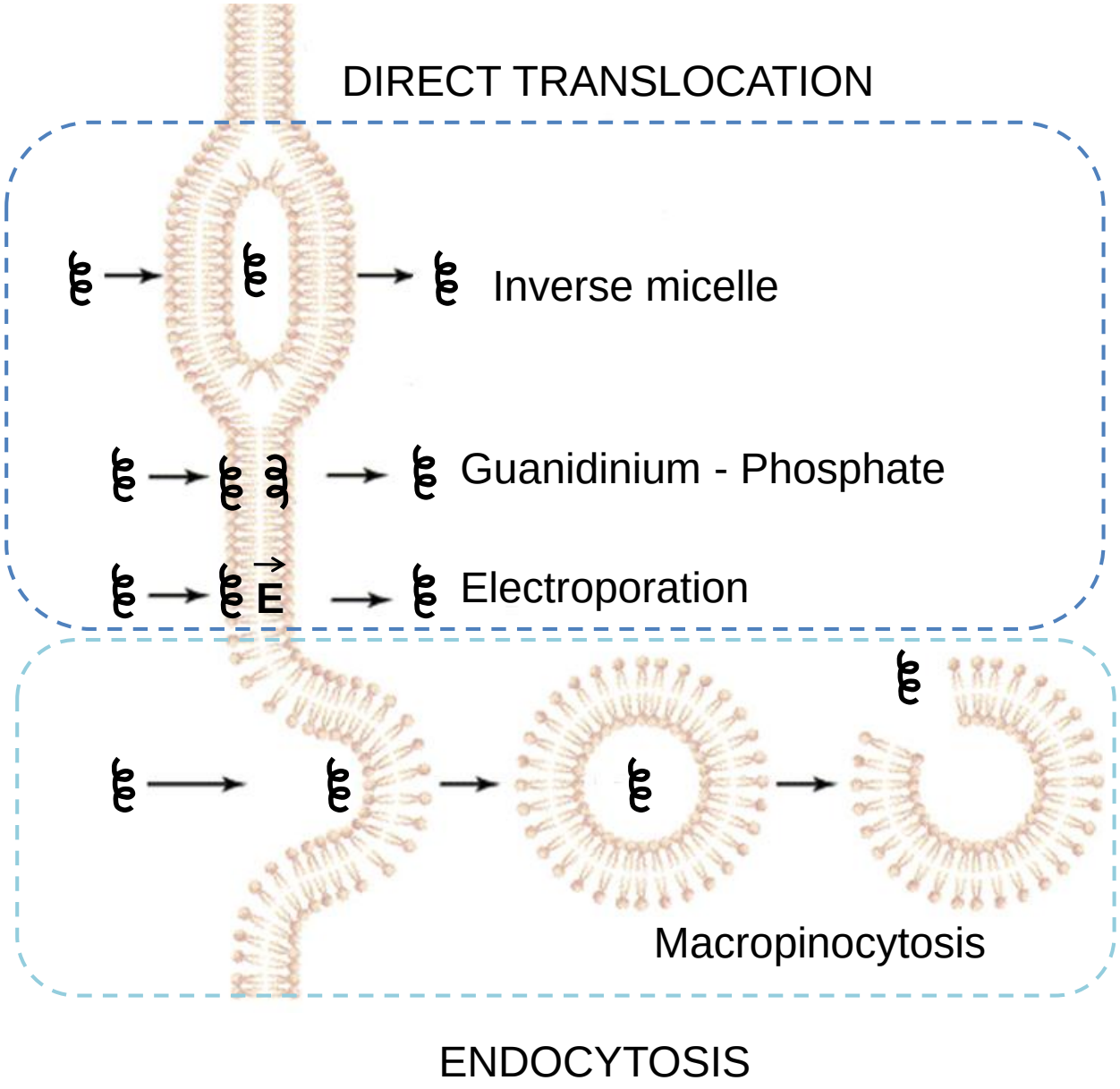

Figure 1. Proposed mechanisms used by penetrating peptides to cross membranes. Image adapted from Sebbage, et al.[9]

A target of particular interest is the mitochondria, due to its role in apoptosis and energy production and subsequently, disease.[14-20] Mitochondrial defects have been attributed to several conditions such as cancer,[21-22] hypothyroidism,[23-25] heart disease,[26-28] and genetic diseases such as MELAS syndrome.[29] Unfortunately, targeting the mitochondria has proven difficult due to the intricacies involved in crossing three membranes: the plasma membrane, along with both the outer and inner mitochondrial membranes (OMM and IMM, respectively) to reach the matrix where energy production and apoptosis take place (Figure 2).[18]

The most difficult barrier to gain access to the matrix is the IMM, which differs significantly from almost all other eukaryotic plasma membranes. In the past, this organelle has been inaccessible by targeted drugs due to the following properties, hindering treatment of mitochondrial diseases.[14-15,17] The IMM has a transmembrane electrochemical potential ($\Delta\psi$) of -180 mV (negative inside), much greater than the transmembrane potential across the plasma membrane of -60 mV.[18] Furthermore, the "signature lipid of mitochondria" is cardiolipin.[18] Cardiolipin is rarely found in other lipid membranes and is a unique phospholipid in that the headgroup is tailored to support four fatty acid tails instead of two.[18] Due to the prevalence of cardiolipin surrounding protein complexes in the electron transport chain embedded in the IMM, it is believed to be essential for the assembly of these complexes or necessary to maintain their functional conformation by acting as a proton trap.[18] This theory is supported by experiments in which the biosynthesis of cardiolipin was inhibited, resulting in mitochondrial defects in respiration.[18] Due to the fact that cardiolipin restricts the permeability of even protons, gaining access to this organelle has proven especially difficult.

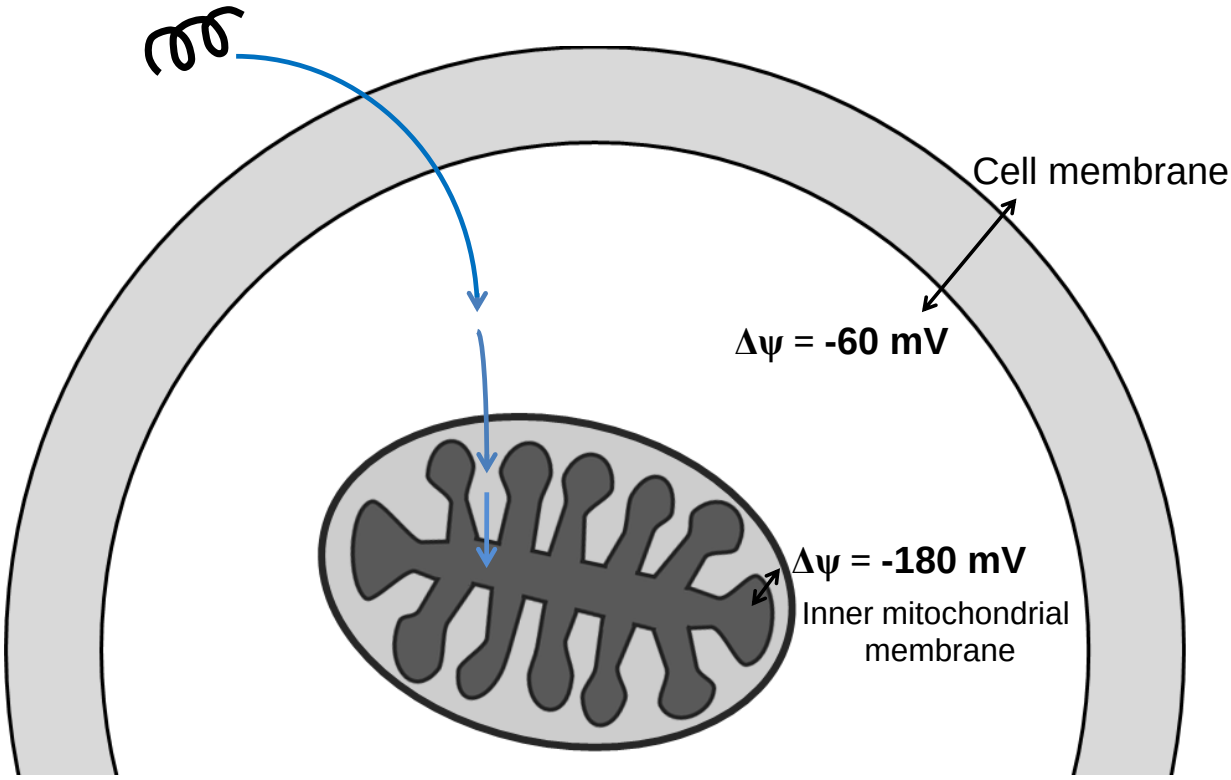

Figure 2. Membrane barriers encountered by mitochondria-penetrating peptides. Cell penetrating peptides only cross the plasma membrane. Mitochondria-penetrating peptides must cross a total of three membrane barriers; the plasma membrane, the OMM, and the IMM. The IMM is the least permeable barrier, with the dense bilayer structure.

In spite of these difficulties, the Kelley group at the University of Toronto was able to design and synthesize a group of peptides that exhibited mitochondrial penetrating properties.[16] Not only are the mitochondria-penetrating peptides (MPPs) able to cross the plasma membrane, once in the cytosol they are able to localize in the mitochondria.[16] MPP uptake and localization was analyzed in a variety of human cell lines by flow cytometry and confocal fluorescence microscopy.[16] By conjugating the MPPs to a fluorophore and comparing with Mitotracker CMXRos (a fluorophore known to localize in the mitochondria), the fluorescence images provided relative mitochondrial specificity.[16]

The Kelley group also examined different mechanisms of internalization. They found that endocytosis inhibitors did not alter the localization, so an energy-dependent mechanism was ruled out.[16] Also, when the transmembrane potential was depleted the MPP uptake decreased.[16] Similarily, when the transmembrane gradient was larger, the MPP uptake was enhanced.[16] These results indicate that MPPs localize in the mitochondria by direct potential-driven diffusion, but the exact mechanism remains unknown.[16] It is also difficult to determine the exact suborganellar location of the MPPs.[16] Due to the resolution limit of confocal microscopy, the outer and inner membranes cannot be resolved and it is impossible to determine whether the MPPs actually reach the matrix.[16]

To achieve atomic-scale resolution, we have used a solid state nuclear magnetic resonance (ssNMR) technique. For our study, we chose a peptide with high mitochondrial localization and the amino acid sequence Cha – Arg – Cha – Lys, where Cha = cyclohexylalanine.[16] With ssNMR we wanted to examine the presence of peptide-induced

changes in membrane structure and morphology. We also used this method to determine the peptide location in our system during translocation.

Model membrane systems are advantageous for research purposes because they accurately mimic biological membranes.[30] With model membranes, we can focus on peptide-lipid interactions and eliminate the complexities present in biological cells, such as carbohydrates and proteins. In order to make a bilayer system that accurately models the IMM, we needed a complex lipid mixture. As with any other membrane, the composition of the IMM varies with respect to tissue type and organism. Three major phospholipids (Table 1) are always present in the IMM at the following percentages: cardiolipin (10-20%), phosphatidylethanolamine (20-40%), and phosphatidylcholine (35-50%).[18] Other phospholipids, such as phosphatidylinositol are generally only present at approximately 5% of total lipid composition along with trace amounts of cholesterol.[18] For this reason, other phospholipids and cholesterol were not part of the composition for the model membrane systems. We used a lipid mixture of 10 mol% cardiolipin, 50 mol% phosphatidylcholine, and 40 mol% phosphatidylethanolamine (Table 1, Figure 3)

Several systems have been developed to model lipid membranes: supported lipid bilayers (SLBs),[31] multilamellar vesicles (MLVs),[32] and giant, large, and small unilamellar vesicles (GUVs,[33] LUVs,[34] and SUVs[35]). For the present study, large unilamellar vesicles were chosen as the model system because they are unilamellar, highly stable,[36] and can be studied with ease using ssNMR. Examination of the orientation and insertion, lipid interaction, and oligomeric structure in similar experiments has led to conclusions about the mechanism of different classes of penetrating peptides.[37]

Table 1. Lipid composition of the inner mitochondrial membrane and our models.

Lipid	Inner mitochondrial membrane	Our model membranes
Cardiolipin (CL)	10-20%	10%
Phosphatidylcholine (PC)	35-50%	50%
Phosphatidylethanolamine (PE)	20-40%	40%
Phosphatidylinositol (PI)	5%	None
Cholesterol	Trace amounts	None

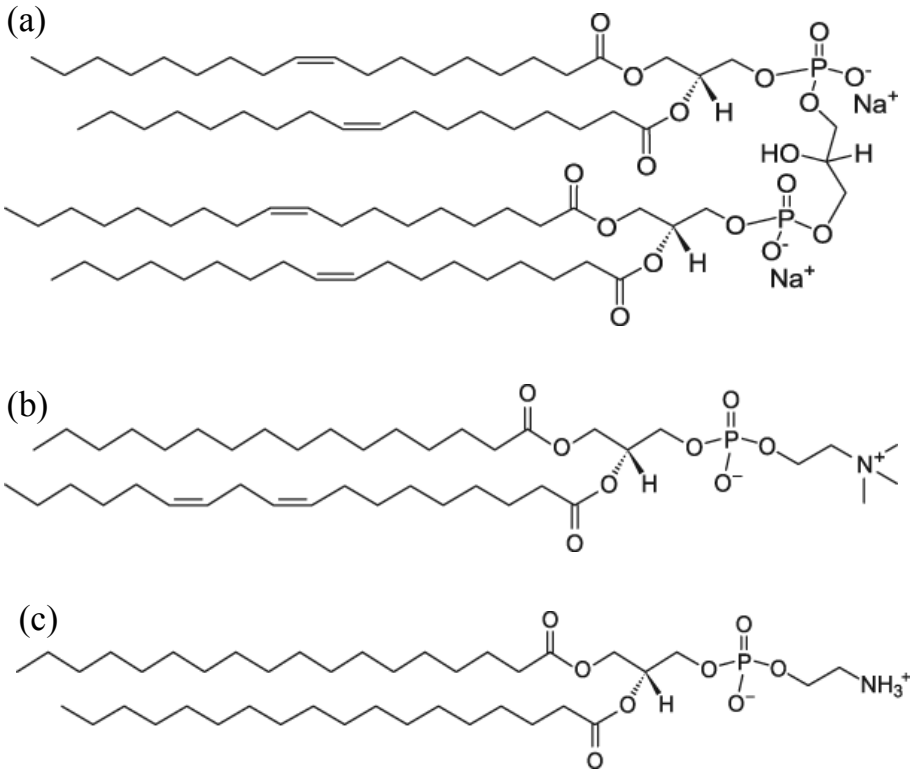

Figure 3. Chemical structures of lipids. (a) Cardiolipin 18:1, (b) Phosphatidylcholine 16:0-18:2, (c) Phosphatidylethanolamine 18:0.

Solid-state NMR (ssNMR) offers the ability to look at MPPs in the lipid bilayer where the mechanism of translocation can be revealed. With ssNMR, we can observe chemical shift anisotropy (CSA) of the phospholipid head groups.[38] The magnitude of the chemical shift will vary as a function of molecular orientation with respect to the magnetic field, which results in the CSA.[38] The chemical shift tensor is expressed in a coordinate frame where the off-diagonal components vanish and only the principal axis system is left.[38] The chemical shift tensor is then described by the principal components: δ_{11}, δ_{22}, and δ_{33} (Figure 4).[38-39] The relative isotropic value associated with these chemical shift tensors is the average of the three:

$$\delta_{iso} = \frac{\delta_{11} + \delta_{22} + \delta_{33}}{3}$$

In this system, the principal component δ_{11} corresponds to the direction of least shielding and highest frequency, while δ_{33} corresponds to the direction of highest shielding and lowest frequency.[40] The anisotropic part of the chemical shift frequency for an axially symmetric shielding tensor is

$$\omega_{cs}^{aniso}(\theta) = -\omega_0 \Delta \frac{1}{2}(3cos^2\theta - 1)$$

where Δ is the CSA.[38,41] For the non-axially symmetric case, the chemical shift frequency can be expressed in terms of the isotropic component, shielding anisotropy, and asymmetry (ε):

$$\omega_{cs}(\theta, \varphi) = -\omega_0 \delta_{iso} - \frac{1}{2}\omega_0 \Delta(3cos^2\theta - 1 + \eta sin^2\theta cos2\varphi)$$

where $-\omega_0\delta_{iso} = \omega_{iso}$ is the isotropic chemical shift frequency, relative to the Larmor frequency, ω_0.[41]

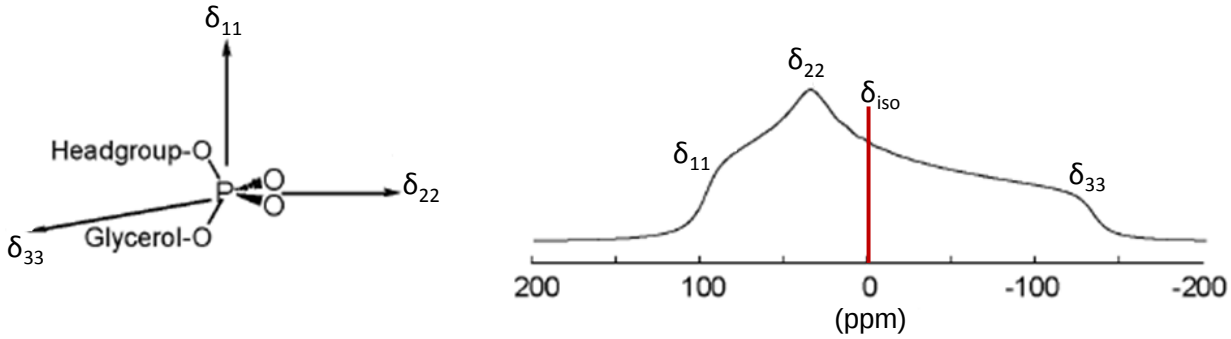

Figure 4. The ^{31}P chemical shift anisotropy of unoriented static phospholipids and the associated chemical shift tensors.[39]

Table 2. The expected NMR results associated with each mechanism of translocation.

Mechanism	NMR Experiment	Expected results
Endocytosis	Static ^{31}P NMR	Changes in ^{31}P CSA, isotropic peaks
Inverse micelles	Static ^{31}P NMR	Isotropic ^{31}P peak in CSA
Guanidinium - Phosphate	PRE ^{13}C MAS NMR	High signal intensity in one side Mn^{2+} bound samples and low signal intensity for two side Mn^{2+} bound samples at all peptide concentrations.
Electroporation	PRE ^{13}C MAS NMR	High signal intensity in one side Mn^{2+} bound samples and low signal intensity for two side Mn^{2+} bound samples at high peptide concentrations. No change in signal intensity between one and two side bound samples at low peptide concentration.

In an unoriented, large unilamellar vesicle system, all molecular orientations are present, so we expect to see a powder pattern (Figure 4).[41] In our sample, the shielding principal axis frame is fixed in the molecule so all values of the angle ζ, and φ in non-axial symmetry, are possible.[41] Each molecular orientation possesses a different orientation on the principal axis frame with respect to the magnetic field, so each has a different chemical shift.[41] The peaks from the different orientations overlap and form a continuous line shape. Some orientations have the same chemical shift, so the resulting intensity at any given frequency in a powder pattern reflections the number of orientations with the same chemical shift.[41] This gives the powder pattern a distinct shape which depends on the symmetry at each nucleus.

In our system, static ^{31}P CSA can be used to observe how the phospholipid headgroups change when bound to the MPP. If the peptide is causing lipid rearrangement, such as endocytosis or inverse micelles, changes in the ^{31}P chemical shift anisotropy would be expected (Table 2).[42] Herein, we present a variable temperature study which examines the powder pattern resulting from the ^{31}P CSA of the both the unbound and MPP bound membrane.

The development of magic angle spinning (MAS) and specialized 2D pulse sequences has led to high resolution spectra, comparable with solution state NMR, which can provide details on the structure and dynamics of a variety of biomolecules.[38,43-44] By spinning at the magic angle of 54.74°, the dipolar coupling quantity in the spin NMR Hamiltonian is reduced to zero, eliminating the anisotropic solid state interactions.[43-44] We use MAS to probe molecular details of our membrane bound MPP system. We use isotropic ^{13}C chemical shift to determine insertion depth.[13,45]

Paramagnetic relaxation enhancement (PRE) experiments were performed to determine which leaflet of the bilayer the MPP interacts and depth of insertion. These properties were investigated by using a ^{13}C MAS NMR PRE method described by the Hong group.[13] Paramagnetic ions are able to bind to membranes and cause line broadening and signal decrease in NMR spectra by enhancing the T_2 relaxation rate.[13] Due to the fact that Mn^{2+} ions cannot penetrate the hydrophobic portion of the bilayer, this PRE effect is distance dependent.[46] The paramagnetic contribution to dipolar transverse relaxation depends on the average electron – nucleus distance (r) according to the following equation[45]:

$$\frac{1}{T_2^P} = W\frac{1}{15}\left(\frac{\mu_0}{4\pi}\right)^2\frac{\gamma_c{}^2\mu_{eff}^2\beta^2}{r^6}\left(4\tau_s + \frac{3\tau_s}{1+\omega_c^2\tau_c^2} + \frac{13\tau_s}{1+\omega_e^2\tau_c^2}\right)$$

where the correlation time τ_s is the inverse sum of the electronic spin-lattice relaxation time T_{1e}, the rotational correlation time of the molecule τ_r, and the residence time of the Mn^{2+} near the nuclear spin τ_m[45]:

$$\frac{1}{\tau_s} = \frac{1}{T_{1e}} + \frac{1}{\tau_r} + \frac{1}{\tau_m}$$

In the first equation, W is the local concentration of Mn^{2+} ions, γ_c is the gyromagnetic ratio of the ^{13}C spin, μ_0 is the vacuum permeability, μ_{eff} is the effective magnetic moment of Mn^{2+} ions, β is the Bohr magneton, ω_c is the ^{13}C Larmor frequency, and ω_e is the electron Larmor frequency.[45] From these equations we can see that the signal attenuation due to the paramagnetic ions is distance dependent.

In this experiment, we can compare the peptide and lipid signal attenuation to determine bilayer sidedness and depth of insertion. For example, a peptide present only in the outer leaflet should have little intensity change between the one side and two side Mn^{2+} bound membranes.[13]

On the other hand, a peptide inserted in both the inner and outer leaflet should have an intensity decrease from one side to two side Mn^{2+} bound samples (Figure 5).[13] By gaining information on the peptide location in the bilayer we can make conclusions about the mechanism of translocation (Table 2).

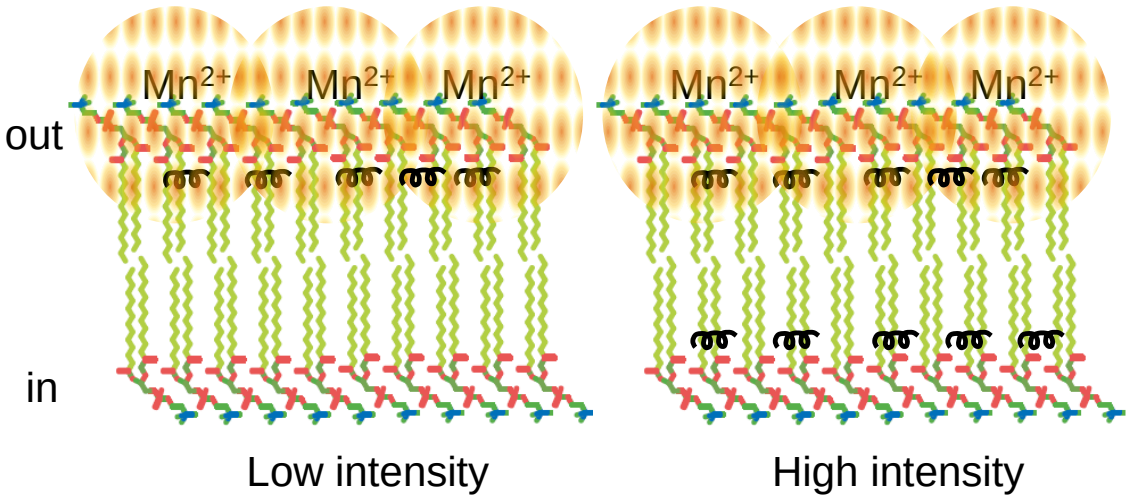

Figure 5. Paramagnetic relaxation effect of Mn^{2+} on peptides in lipid bilayers. Peptide bound to only the outer leaflet will exhibit low NMR intensity in the one side Mn^{2+} bound sample (left). Peptide bound to both bilayers will retain high intensity from peptide signals from the inner leaflet unaffected by the one side nature of Mn^{2+} (right).

2.0 MATERIALS AND METHODS

Lipids and Peptides

All lipid products used to form the model mitochondrial membranes are commercially available, including 1,1',2,2'-tetraoleoyl cardiolipin sodium salt (18:1 CL), 1-palmitoyl-2-linoleoyl-*sn*-glycero-3-phosphocholine (16:0-18:2 PC), and 1,2-distearoyl-*sn*-glycero-3-phosphoethanolamine (18:0 PE), and were purchased from Avanti Polar Lipids, Inc. (Alabaster, AL) and used without further purification. The MPP under investigation (Cha – Arg – Cha – Lys) was purchased from AnaSpec, Inc. (Freemont, CA) with uniformly labeled ^{13}C, ^{15}N residues at positions R2 and K4 at > 95% purity. Unlabeled peptide was also purchased from GenScript Corporation (Piscataway, NJ). All other chemicals were purchased from Thermo Fisher Scientific (Pittsburgh, PA) and used as received.

Large Unilamellar Vesicles

Hydrated CL/PC/PE membranes were formed by dissolving the lipids in chloroform or a 95:5 benzene:ethanol mixture at an appropriate molar ratio of 0.1/0.5/0.4, respectively. The lipid mixture was dried under a stream of nitrogen gas and placed on a vacuum pump overnight to remove residual solvent when chloroform was used, or lyophilized overnight when the benzene:ethanol mixture was used. The dried lipid cake was rehydrated with a suitable buffer,

either 10 mM acetate buffer at pH 6 or 10 mM phosphate buffer at pH 7 and heated to 85°C. The particular buffer composition was used to avoid interference in the ^{13}C and ^{31}P NMR signals, respectively. The rehydrated lipid sample was incubated for 2 hours at 85°C and vortexed periodically to produce MLVs. The sample was heated to 85°C so that extrusion was performed above the highest transition temperature, T_m, of the lipid mixture. The resulting MLVs were converted to LUVs using a mini extruder (Avanti Polar Lipids, Inc.) and passed through a 100 nm polycarbonate membrane 21 times to produce homogeneous vesicles with a diameter of 100 nm. The size of the vesicles was validated by dynamic light scattering on a ZetaPALS particle size analyzer. From this point forward, the LUVs were kept at 37°C to maintain a physiologically relevant temperature. The MPP was added to the LUV solution and incubated overnight. The LUVs were centrifuged at 150 000*g* for 2.5 hours to yield a hydrated membrane pellet, which was packed into a 200 μL MAS rotor.

Some of the experiments also incorporated Mn^{2+} as a paramagnetic relaxation enhancement agent. For these samples, the Mn^{2+} solution was prepared from $MnCl_2 \cdot 4H_2O$ and added at 8 mol% of the lipids. To obtain one side Mn^{2+} bound vesicles, the Mn^{2+} solution was added after ultracentrifugation, typically directly to the rotor containing unbound vesicles. The one side Mn^{2+} bound vesicles were freeze-thawed 8-10 times, creating MLVs with Mn^{2+} on both sides.[13]

LUVs Exhibiting a Transmembrane Potential

In an attempt to more accurately model mitochondrial membranes, we constructed LUVs with a transmembrane gradient following a protocol developed by the Hope group.[47] The Hope protocol states that by entrapping high buffer concentration in LUVs, a negative gradient can be formed

across the membrane by having an acidic pH inside and a neutral pH outside.[47] Membranes are extremely permeable to H^+ ions, but this process is self limiting because the efflux of H^+ also sets up a positive electrical potential outside of the membrane, which inhibits H^+ ions from leaving the interior.[47] At equilibrium, the potential of the membrane will follow the Nernst equation:

$$\Delta\psi = -59 \log \frac{[H^+]_{in}}{[H^+]_{out}}$$

Therefore, if the membrane is constructed with pH 4 inside and pH 7 outside, the membrane will exhibit an electrochemical potential of -177 mV,[47] which is close to the true mitochondrial gradient of -180 mV.[18] The existence of a three unit pH gradient in our system was confirmed by the fluorescence response of 9-aminoacridine as described by Casadio and Melandri.[48]

Hydrated membrane samples were formed as previously described with a few minor changes to establish the gradient. For example, the lipid cake was rehydrated with 300 mM phosphate buffer at pH 4 to ensure the stability of the gradient and produce an acidic interior. The rehydrated sample was extruded in the same manner. However, after extrusion, the LUVs were dialyzed overnight using a Slide-A-Lyzer (Thermo Fisher Scientific) to remove the higher density, more acidic buffer and replace it with 10 mM phosphate buffer at pH 7 for the exterior membrane environment. In MPP incorporated samples, the peptide was added after dialysis and ultracentrifuged. All other experimental parameters and consequent steps were the same as previously described in Section 2.1.3.

To produce one side Mn^{2+} bound vesicles, the lipids were extruded with 8 mol% Mn^{2+} and then dialyzed, resulting in vesicles with Mn^{2+} bound to only the inner leaflet. To produce two side Mn^{2+} bound vesicles and maintain the gradient, the freeze-thaw method could not be

used. This procedure disrupts the unilamellar lipid bilayer by reassembling the lipids through ice formation. Therefore, the vesicles with Mn^{2+} bound to only the inner leaflet had 4 mol% Mn^{2+} added to the membrane pellet to produce two side Mn^{2+} bound LUVs.

NMR Spectroscopy

All NMR measurements were carried out on a Bruker Avance 500 (11.7 T) spectrometer at a resonance frequency of 500 MHz for ^{1}H, 200 MHz for ^{31}P, 125 MHz for ^{13}C, equipped with a BCU05 Variable Temperature Control Unit. Data was processed using Bruker Topspin 1.3 or iNMR software. All sample rotors were Bruker 4 mm ZrO_2 magic angle spinning (MAS) rotors with internal volumes of 12 μL, 50 μL, or 200 μL. All experiments were performed using a Bruker HXY broadband MAS probehead doubly tuned to $^{1}H/^{13}C/Y$ or $^{1}H/^{31}P/Y$. ^{13}C chemical shifts were externally referenced to adamantane at 38.5 ppm on the TMS scale. ^{31}P chemical shifts were referenced to 85% phosphoric acid at 0.0 ppm. The spinning rate for MAS experiments was 5 kHz.

Static ^{31}P spectra were decoupled with WALTZ-16 at ^{1}H field strengths of 6 kHz. Typical radiofrequency (rf) pulse lengths were 4 μs for ^{31}P and 1-2 μs for ^{1}H. A minimum of 1200 scans were collected, each consisting of 4096 complex data points. ^{31}P spectra were acquired using an inverse-gated pulse sequence. The acquisition time was 68 ms, spectral width was 30 kHz, the recycle delay was 3 s, and the sample volume was 50 μL.

^{13}C direct polarization MAS NMR spectra were decoupled with two pulse phase modulation (TPPM) at ^{1}H field strengths of 30 kHz. Typical radiofrequency (rf) pulse lengths were ~5 μs for ^{13}C and 1-2 μs for ^{1}H. A minimum of 6144 scans were collected, each consisting of 8192 complex data points. ^{13}C spectra were acquired using an inverse-gated pulse sequence

for direct polarization. The acquisition time was 41 ms, spectral width was 50 kHz, the recycle delay was 8 s, and the sample volume was 200 μL.

3.0 RESULTS AND DISCUSSION

Membrane Morphology in the Presence of Peptide

Static ^{31}P NMR spectra show the chemical shift anisotropy (CSA) of solids and can provide information on the structure and phase behavior of phospholipid headgroups. In this experiment, we vary the temperature over a wide range from 280 K – 360 K (the highest phase transition temperature of the lipid mixture is 347 K). First, a series of variable temperature experiments were collected for the CL/PC/PE LUVs in the absence of peptide to ascertain the behavior of the pure membranes. These results are compared in Figure 6 to MPP-containing membranes with a high peptide to lipid ratio of 1:12.5. If the MPP is perturbing the dynamics of the membrane, it would be apparent at high peptide to lipid ratios. However, in all spectra, we observed a powder pattern, characteristic of undisrupted, unoriented LUVs. The lack of an isotropic signal at 0 ppm rules out the possibility of inverse micelles shuttling the peptide into the cell.

Overall, from this data, we were able to conclude that aside from extremely small differences, the ^{31}P CSAs show generally the same powder pattern in the presence of the MPP. Also, the same spectra are observed before and after the phase transition. This indicates that the peptide does not alter the phase behavior of the lipids or cause membrane disruption. Therefore, the MPP most likely does not translocate via an energy dependent mechanism, such as

endocytosis. This observation is consistent with the theory that MPPs translocate without damaging the integrity of the membrane.

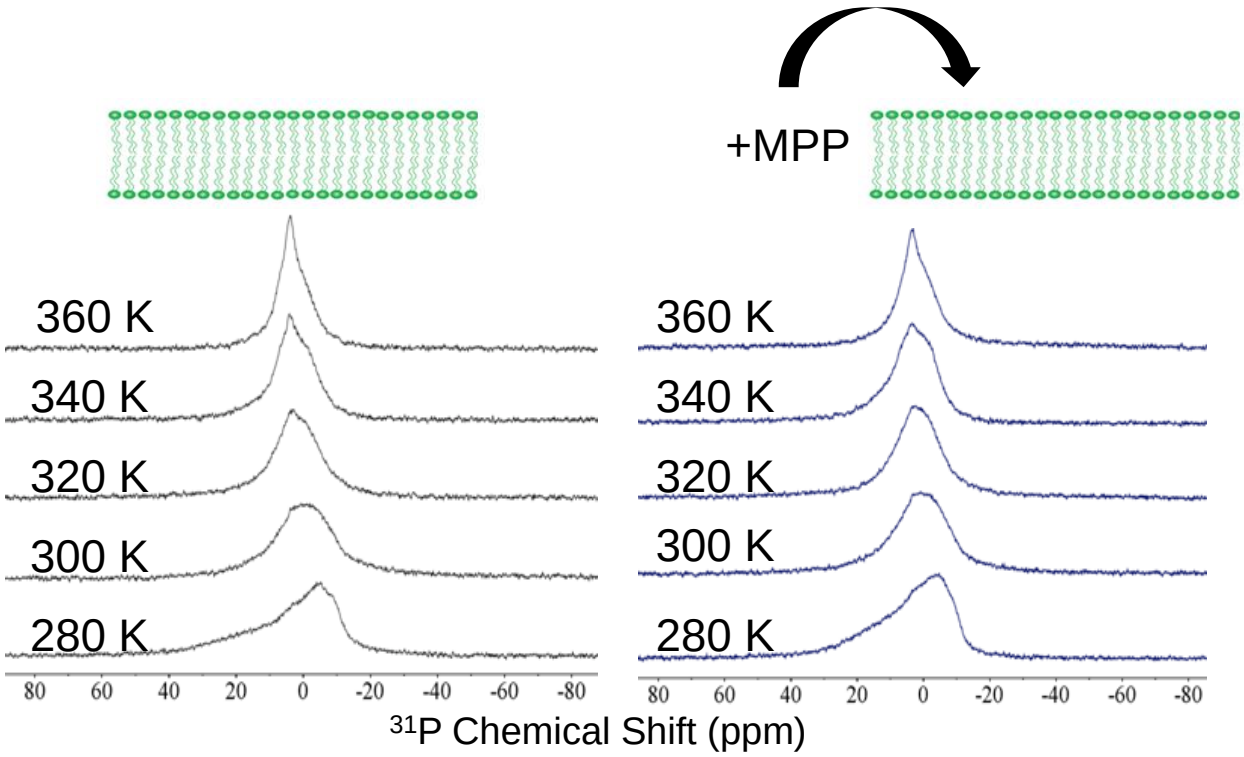

Figure 6. The peptide does dramatically alter the structure of the membrane. Static ^{31}P NMR spectra of liposomes (a) in the absence of MPP and (b) in the presence of MPP.

Location of Peptide in the Bilayer

Since preliminary evidence suggested a mechanism of direct translocation for the MPP, we decided to test the hypothesis of electroporation by PRE with Mn^{2+} to determine the depth of insertion. First, we had to establish that our lipid membrane system could confine paramagnetic ions to one side of the bilayer for asymmetric measurements. In order to confirm the one sided binding of Mn^{2+} to CL/PC/PE LUVs, static ^{31}P NMR spectroscopy was performed to examine the dephasing of the headgroups in absence of the MPP. The results are shown in Figure 7 and the one side Mn^{2+} samples show dephasing of 47%, which is reasonable; approximately half of the lipid headgroups from the inner leaflet are not affected by the PRE. As expected, the ^{31}P signal is completely dephased for the two side Mn^{2+} bound samples.

After verifying the one and two side Mn^{2+} distribution across the bilayer, the feasibility of using gradient vesicles was examined. To begin, the MPP was added to both non-gradient and gradient ($\Delta\psi$ = -177 mV) vesicles at a peptide-to-lipid ratio of P:L = 1:40 and probed with ^{13}C direct polarization MAS NMR. In order to compare between different samples, the peak intensity was double-normalized, $(S/S_0)/(S/S_0)_{max}$ where S is the signal intensity of the Mn^{2+} bound sample, S_0 is the signal intensity of the unbound reference sample, and $(S/S_0)_{max}$ is the normalized value of the lipid peak with the least attenuation. The maximum value typically fell between the methyl group at the end of the acyl chain (ω) and the CH_2 groups because they are embedded in the center of the bilayer and experience the least PRE.

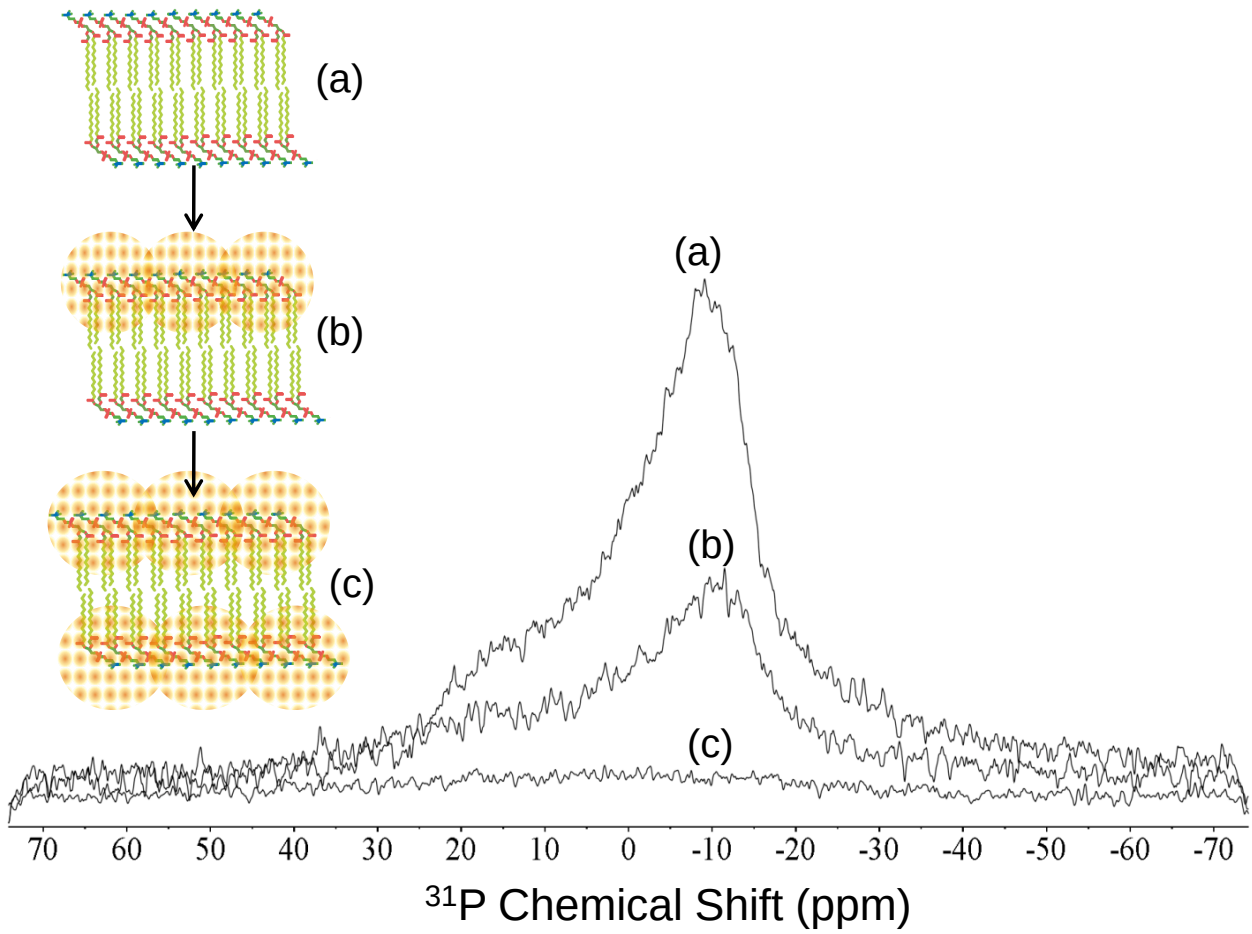

Figure 7. Manganese ions do not cross the bilayer and form stable one side bound samples. Static ^{31}P NMR spectra of (a) unbound, (b) one side Mn^{2+} bound with 47% dephasing, and (c) two side Mn^{2+} bound with 100% dephasing CL/PC/PE LUVs.

According to our results, the lipid peaks are attenuated as expected for all samples. In the one side Mn^{2+} bound samples, much of the signal intensity from the acyl chain is retained at 80 – 100% until C2. At this point, the signal becomes dephased significantly at approximately 40% from C1 through the glycerol and choline peaks. In the two side Mn^{2+} bound samples, the dephasing decreases even more in this region to 0-25%. Upon comparison of the gradient and non-gradient vesicles, nearly identical spectra were observed. As shown in Figure 8, the MPP is only distributed on the outer leaflet of the bilayer and at the same insertion depth between both samples. Therefore, we can conclude that the LUVs exhibiting a gradient of -177 mV are a reliable model to assess the mechanism of MPPs.

To investigate the electroporation model, the MPP was added to the gradient LUVs at both low (P:L = 1:40) and high (1:10) concentrations. Figure 9a-b shows that at P:L = 1:40, the peptide peaks have the same low intensity in the one and two side Mn^{2+} bound samples. This result is indicative of the MPP binding to only the outer leaflet of the bilayer. When the peptide-to-lipid ratio is increased to P:L = 1:10, the peptide peaks experience greater attenuation in the two side Mn^{2+} bound sample (Figure 9d) as compared to the one side Mn^{2+} bound sample (Figure 9c). Therefore, at this ratio the peptide is bound to both the inner and outer leaflet of the bilayer. In the one side Mn^{2+} bound experiment, only half of the MPP is experiencing dephasing due to the PRE, thus maintaining most of its signal intensity. However, in the two side Mn^{2+} bound sample, all of the peptides are subjected to the PRE, resulting in a decrease in intensity as shown by the fractions of intensity indicated below the peptide peaks. Figure 10 shows a graphical representation of the PRE effect on the normalized signal intensity. At low P:L = 1:40, there is no change in signal intensity when comparing one side and two side Mn^{2+} bound membranes. At high P:L = 1:10, the peptide retains much of its signal intensity (about 80%) in

the one side Mn^{2+} bound sample, while in the two side Mn^{2+} bound sample, the signal intensity is significantly lowered (average is approximately 50%). Therefore, we can conclude that at low peptide concentrations, the MPP binds only to the outer leaflet while at high peptide concentrations the MPP is distributed in both the inner and outer leaflet of the bilayer.

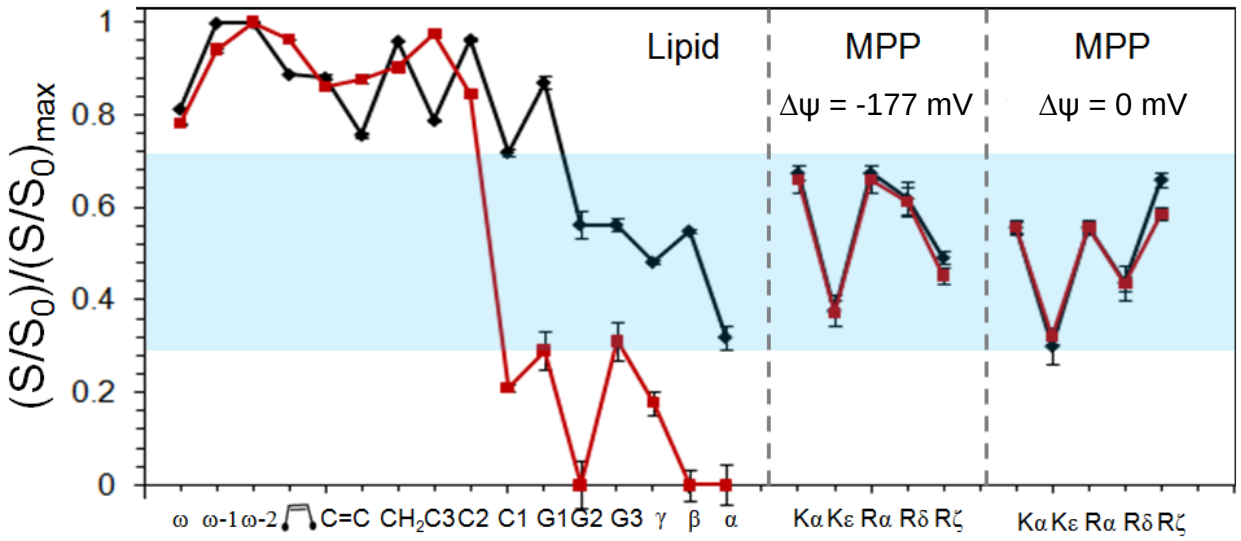

Figure 8. The intensity of the Mn^{2+} bound sample (S) double normalized with respect to the unbound sample (S_0) and the maximum lipid peak $(S/S_0)_{max}$. The shaded region shows the depth of MPP insertion in the bilayer for non gradient (Δψ = 0 mV) and gradient (Δψ = -177 mV) LUVs.

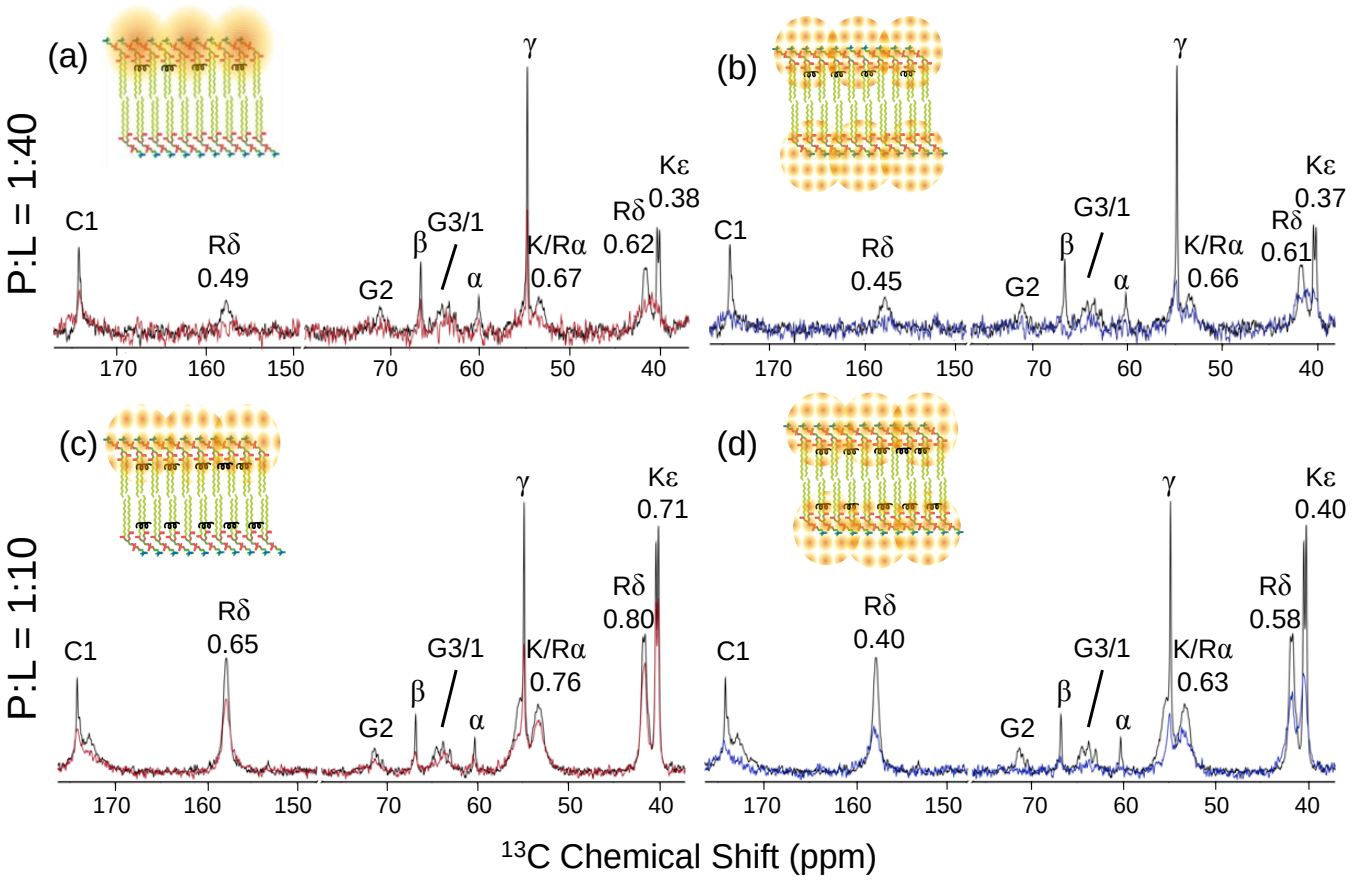

Figure 9. ^{13}C MAS NMR spectra illustrating the attenuation due to the PRE effect at low (P:L = 1:40) and high (P:L = 1:10) peptide concentrations. The membrane schematics indicate the peptide location. a) One side Mn^{2+} bound CL/PC/PE vesicles with P:L = 1:40 red spectra, b) two side Mn^{2+} bound CL/PC/PE vesicles with P:L = 1:40 blue spectra, c) one side Mn^{2+} bound CL/PC/PE vesicles with P:L = 1:10 red spectra, and d) two side Mn^{2+} bound CL/PC/PE vesicles with P:L = 1:10 blue spectra. All spectra are overlaid with the unbound spectra (black) with the percent dephasing displayed for the peptide peaks.

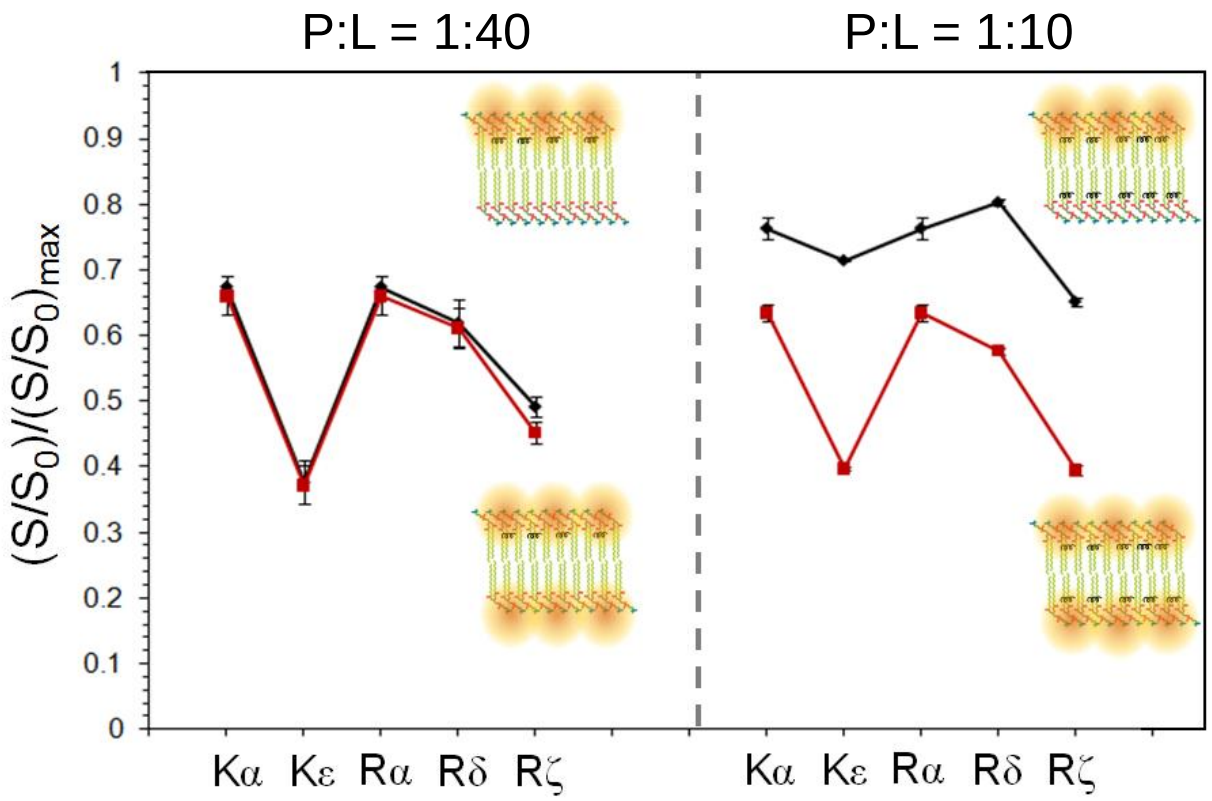

***Figure 10*.** High peptide concentration leads to distribution in both leaflets. At low P:L = 1:40 the MPP only binds to the outer leaflet because there is no change in the signal intensity. At high P:L = 1:10 the one side Mn^{2+} bound sample shows high signal intensity and the two side Mn^{2+} bound sample shows low signal intensity, indicative of distribution in both leaflets.

From this data, it is also possible to estimate the MPP location in the bilayer (Figure 11). For P:L = 1:40, the normalized peptide signals are only compared to the two side Mn^{2+} bound lipid peaks. Because the MPP is only binding to the outer leaflet at this ratio, it is inaccurate to compare the intensity to the one side Mn^{2+} bound lipid peaks because only half of the lipids are experiencing PRE in this instance. Due to the fact that the MPP is fully dephased, all of the lipids must also be fully dephased to estimate the depth of insertion. Figure 10a shows that the MPP is inserted at approximately C1 - C2, at the top of the acyl chain in the interfacial region. This depth agrees with the electroporation model, which states that at low peptide-to-lipid ratios, the cationic side chains of the penetrating peptide interact with negatively charged phosphate headgroups on the outer leaflet.

When the ratio is increased to P:L = 1:10, the peptide is distributed into both leaflets. For the one side Mn^{2+} bound sample, the peptide intensity is directly compared to the one side Mn^{2+} bound lipid signal. In this case, it is assumed that the MPP is distributed evenly on both leaflets and therefore, half of the peptide signal is retained, much like that of the lipid. For the same reason, the two side Mn^{2+} bound peptide intensities are compared to the two side Mn^{2+} bound lipid intensities. From the analysis shown in Figure 11b-c, it was concluded that the MPP is inserted symmetrically into both leaflets in the proximity of C2. Again, the MPP is still near the top of the acyl chain which further supports the electroporation theory. It is believed that anionic lipids, in this case cardiolipin, gather under the cationic peptides bound to the outer leaflet. At a certain threshold, this cationic peptide – anionic lipid system acts as a capacitor with a voltage negative enough to form transient pores, allowing the peptide to cross the bilayer where it can interact with negatively charged phosphate headgroups present on the inner leaflet.

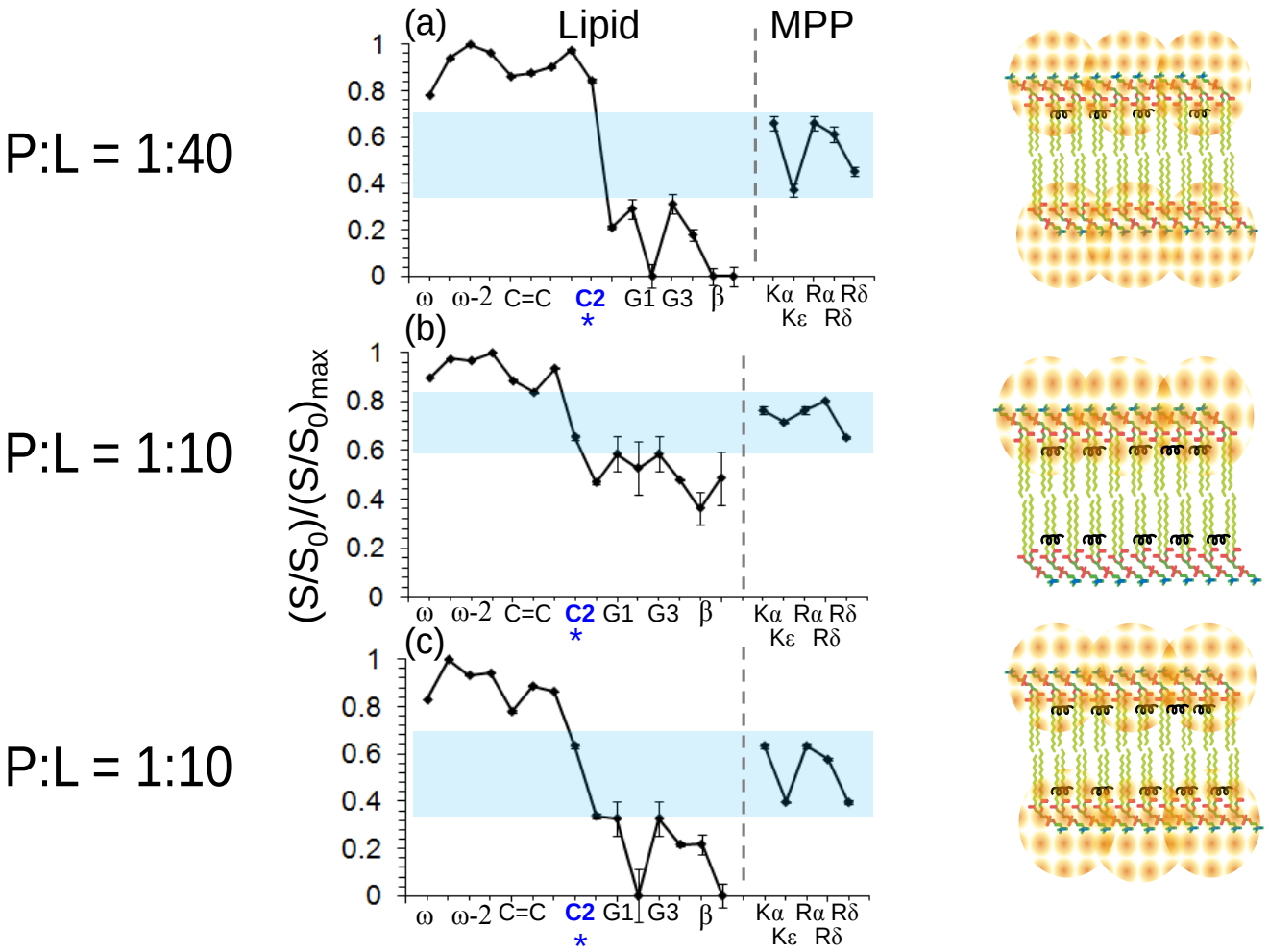

Figure 11. At both high and low peptide concentrations, the MPP is bound near C2 of the lipid acyl chain. The intensity of the Mn^{2+} bound sample (S) double normalized with respect to the unbound sample (S_0) and the maximum lipid peak $(S/S_0)_{max}$. The shaded region shows the depth of MPP insertion in the bilayer for (a) two side Mn^{2+} with P:L = 1:40, (b) one side Mn^{2+} with P:L = 1:10, and (c) two side Mn^{2+} with P:L = 1: 10.

Furthermore, the electroporation model provides an explanation as to how and why MPPs translocate the dense, hydrophobic portion of the inner mitochondrial membrane, which requires crossing an energy barrier higher than the peptide gains from crossing the potential difference of -180 mV present across the membrane. As charged peptides accumulate asymmetrically on the outer leaflet of the bilayer, a transmembrane electric field is induced that disrupts the local bilayer structure.[7,9] In this study, the MPP is a short, four residue peptide with one arginine and one lysine residue, providing two cationic charges that can interact with phosphate headgroups of all three lipids: CL, PC, and PE. The electrostatic potential of a few MPPs binding to the outer leaflet is not strong enough for electroporation because the charge is reduced by counterions and the mean relative permittivity.[8] An adequate amount of MPPs, (i.e. threshold concentration) need to bind nearby to provide the surface charge density to attract negatively charged phospholipids, which are diffusing on the inner leaflet in order to form a capacitor of sufficient voltage to permit passage through the formation of transient pores.[8] The threshold for a sufficient voltage across a capacitor to form pores of electroporation ranges from -250 to -550 mV.[8]

This indicates that the standard voltage observed across mitochondrial membranes is not enough to pull the peptides across, which is in agreement with our system where we observe no translocation (no peptide is reaching the inside of the vesicle). We have established that at high peptide-to-lipid ratios the MPP is pulled into the inner leaflet of the bilayer, but what happens in vivo? To answer this question, we examined two possibilities: (1) the MPP remains trapped in the IMM and does not translocate in vivo and (2) the curvature and salt concentration of our model system does not allow translocation of the MPP.

Free Energy Change of Peptide Translocation

The transmembrane potential across mitochondrial membranes and the previously described model membrane is approximately -180 mV.[18] An average bilayer thickness of our system was calculated to be 4.98 nm, based on literature values of bilayer thickness of cardiolipin,[49] phosphatidylcholine,[50] and phosphatidylethanolamine.[51] From this information, we calculated the electric field across the CL/PC/PE bilayer to be 3.6×10^7 V/m. We then calculated the driving force that this electric field exerts on the MPP using the following equation,

$$F = E \cdot q$$

where F is force, E is electric field across the CL/PC/PE bilayer, and q is the charge of the peptide. From this equation, we found that the force driving the MPP across the bilayer is $F = 1.2 \times 10^{-11}$ J/m or 36 kJ/mol, considering that the peptide has two positively charged residues, Arg and Lys.

At high peptide-to-lipid ratios, we observe distribution of the peptide into both leaflets of the bilayer. It is interesting to consider the energy barriers that the MPP had to overcome in order to go from the outer leaflet, through the hydrophobic center of the bilayer, to the inner leaflet of the bilayer. We have analyzed this translocation as a three step process that is illustrated in Figure 11: (1) insertion into the outer leaflet at the membrane-water interface, (2) insertion into the hydrocarbon core, (3) insertion into the inner leaflet membrane-water interface (Figure 12).

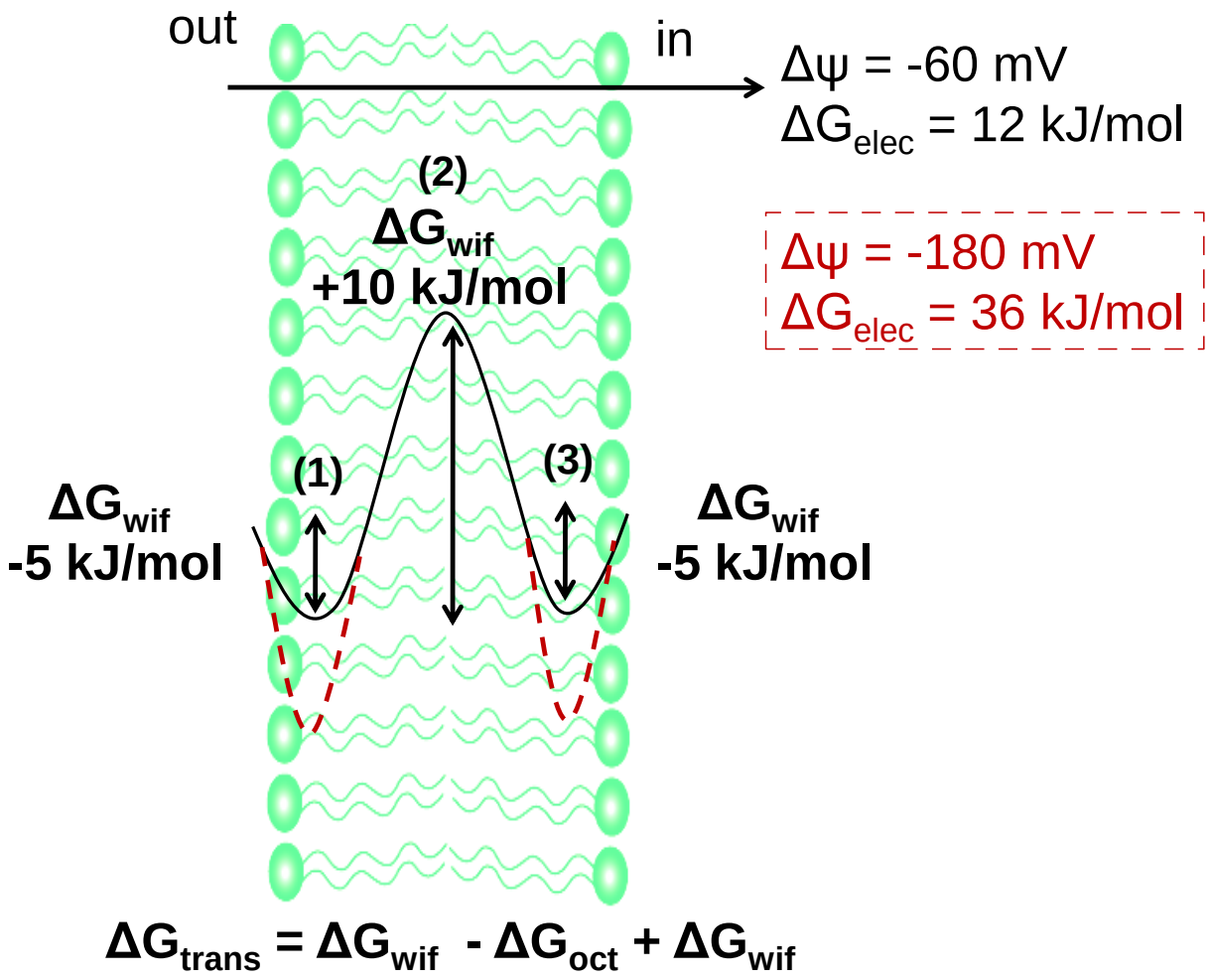

Figure 12. The energy profile associated with inserting the MPP into a plasma membrane (black) and the inner mitochondrial membrane (red). Step 1 inserts the MPP into the interfacial region of the outer leaflet. Step 2 inserts the MPP into the hydrocarbon core of the bilayer. Step 3 inserts the MPP into the interfacial region of the inner leaflet. Crossing the hydrocarbon core is associated with the highest energy barrier. The transmembrane potentials provide a driving translocating force.

The energy cost of inserting the MPP into the outer leaflet at the membrane-water interface (1) was analyzed using the Wimley-White interfacial hydrophobicity scale determined from measurements of short peptides partitioning into zwitterionic phosphatidylcholine (POPC) vesicles.[52-53] Therefore, this calculation reflects the free energy of insertion into zwitterionic vesicles. The equation used to estimate the free energy of insertion from water to interfacial (wif) region is as follows:

$$\Delta G_{wif} = \Delta G_{NH_3^+} + \Delta G_{Phe} + \Delta G_{Arg} + \Delta G_{Phe} + \Delta G_{Lys} + \Delta G_{COO^-}$$

$$\Delta G_{wif} = -3.05\ kJ/mol$$

Although the MPP in consideration has the amino acid sequence Cha – Arg – Cha – Lys, free energy of insertion values are not reported for any unnatural amino. Because Cha closely resembles Phe, this free energy value was substituted to give an estimate. Cha is more hydrophobic than Phe, so we would expect ΔG_{wif} to be slightly greater than the calculated value of -3.05 kJ/mol for the actual MPP sequence. However, we must also consider that each guanidinium ion can form up to five hydrogen bonds with the lipid phosphates or water.[54] If we assume that each hydrogen bond can contribute a favorable free energy change of -2.09 kJ/mol,[55] then the free energy change could be as low as -5.14 kJ/mol. Therefore, we will assume that insertion of the MPP into the interfacial region is a favorable process.

For the second step, insertion of the MPP into the hydrocarbon core of the bilayer, we estimated the free energy barrier using the Wimley-White octanol hydrophobicity scale determined from measurements of short peptides partitioning from water into *n*-octanol (woct).[56] The equation used to estimate the energy of insertion into the hydrophobic core is as follows:

$$\Delta G_{woct} = \Delta G_{Phe} + \Delta G_{Arg} + \Delta G_{Phe} + \Delta G_{Lys} + \Delta G_{Hbond\ per\ residue}$$

$$\Delta G_{woct} = 13.35\ kJ/mol$$

The additional value ΔG_{Hbond} must be included to account for the cost of partitioning a hydrogen bonded peptide backbone into the hydrophobic core.[56] For our purposes, we have estimated this value to be +2.09 kJ/mol.[56] Again, the free energy value for Phe was used in place of Cha to estimate the energy of insertion into the hydrophobic core. Because Cha is more hydrophobic than Phe, we expect the actual free energy of insertion to be more favorable than the estimated value of ΔG_{woct} = 13.35 kJ/mol.

To ensure that this energy barrier to cross the hydrophobic core was reasonable, we compared the estimated ΔG_{woct} to a similar calculation based on an experiment performed by the Kelley group to estimate lipophilicity.[16] A modification of the shake-flask method previously described[57] was used to determine the octanol partitioning of the MPP conjugated to thiazole orange and was reported as the partition coefficient, *log P* = -1.1.[16] From this value the free energy from aqueous solution to octanol can be computed by the following equation:

$$\Delta G = -2.303RT\,logP$$

where *R* is the gas constant and *T* is temperature. This equation estimates the free energy of insertion to the hydrocarbon core to be 6.5 kJ/mol at physiological temperature, which is about half of the previous estimate of 13.35 kJ/mol. Some discrepancies are expected to arise from the Phe substitution for Cha and the conjugation of thiazole orange onto the MPP. Thiazole orange is a large, organic molecule and Cha is more hydrophobic than Phe, so it is logical that the free energy is much lower than the estimated value. Therefore, an average estimate for the energy

barrier that the MPP has to overcome to cross the hydrophobic core of the IMM is approximately 10 kJ/mol.

Since we expect the interfacial region of the outer leaflet to be the same environment as the inner leaflet, the estimated value of ΔG_{wif} = -5 kJ/mol will be the same for the third step as for the first step. If we examine the force across the plasma membrane, F = 12 kJ/mol (Figure 12), this force is sufficient to pull the cationic peptide across the free energy barrier in the hydrocarbon core and overcome the stabilizing forces present in the interfacial region to enter the cytosol. From here, the peptide will be pinned down by the electric field outside the outer mitochondrial membrane. The OMM contains pore-like structures call porins, which all the passage of small peptides.[18] The peptide can electrostatically interact with the anionic inner mitochondrial membrane.

However, the process that occurs in the inner mitochondrial membrane is unclear. Because the inner mitochondrial membrane is anionic, rather than zwitterionic, the favorable free energy associated with the water – membrane interface will be lower than the calculated values (dotted red lines in Figure 12). This is due to the fact that the peptide experiences less charge – charge respulsion from a positively charged choline or ethanolamine headgroup. Although the force exerted by the transmembrane potential (36 kJ/mol) is about three times greater than that of the plasma membrane, it may not be enough to remove the peptide from the interfacial region and into the matrix because we do not know the depth of the wells. But, if the transmembrane gradient is the only force acting on the peptide, it is enough to pull the peptide over the high free energy barrier of the hydrocarbon core (we see distribution in both leaflets at high peptide concentration), it is likely enough to translocate from the interfacial region to the matrix. We can conclude that translocation of the peptide across the plasma and inner mitochondrial membrane

is a favorable process. Therefore, we probably do not observe translocation due to our system limitations.

A viable reason that the MPP remains trapped in our model mitochondrial membranes is that the curvature strain, exacerbated by the presence of cardiolipin, and the salt concentration are preventing translocation. The curvature dependence on translocation of penetratin has been examined in other works with some conflicting results.[58-59] One study showed that penetratin readily crosses GUVs (diameter >1 μm), but remain trapped in the lipid bilayer of LUVs (diameter 100 nm), indicating that curvature can dictate translocation.[58] However, other work showed that in the presence of a transmembrane potential of -110 to -130 mV, penetratin was able to translocate across LUVs with a variety of lipid compositions, indicating that a transmembrane gradient allows the peptide to overcome the barrier of curvature strain.[59] In our system we observe distribution of the MPP into both leaflets at high peptide concentration, but have not seen full translocation.

The curvature strain present in LUVs has caused CPPs to become trapped in the bilayer,[58] and our system contains a lipid composition that lends itself to additional curvature. Cardiolipin, in particular, has been associated with stabilizing curvature in GUVs[60-61] as well as LUVs.[60] In the presence of local acidic pH, vesicles containing cardiolipin were shown to deform in such a way that mimicked cristae (Figure 13), the folds found biologically in mitochondria.[60] It is possible that the acidic pH encapsulated in our model LUVs is acting as a local addition of acidic pH and is causing membrane deformations, similar to those shown in Figure 13. If this is the case, the curvature strain affecting our system would be much more substantial than the curvature normally encountered in LUVs and could be preventing translocation of the MPP. Although changing our membrane composition is not an option because cardiolipin plays such a

vital role in the IMM,[18] the Kelley group has shown that the MPP is able to translocate across the plasma membrane in live cells in order to localize in the mitochondria.[16] It would be of interest to determine how the MPP interacts with a model plasma membrane to see what insights this could provide for the mechanism of mitochondrial localization.

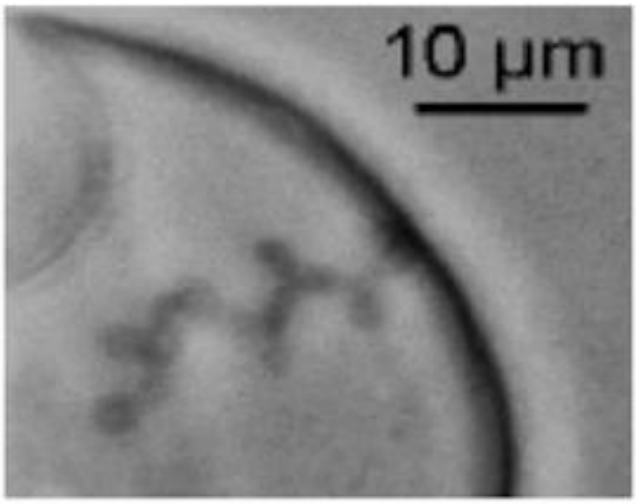

Figure 13. Cristae-like invaginations that are formed in GUVs with the local addition of HCl (100 mM, pH 1.6).[62]

Another factor that could be influencing the translocation of the MPP is the high salt concentration, 300 mM, inside our LUVs to establish a transmembrane gradient of -180 mV. In the study that showed that CPPs can translocate across LUVs in the presence of a transmembrane potential, a different technique was used to establish the gradient.[59] To construct a potential of -110 to -130 mV, Terrone and coworkers used a buffer concentration of only 128 mM KCl and added of valinomycin, which selectively pumps K^+ ions out from inside the LUV to make the inside negative.[59] The membrane binding of peptides is extremely sensitive to salt concentration. In a study examining the thermodynamics of polylysine binding to lipid membranes, the free energy of binding decreased from -1.5 to -7 kcal/mol when the salt concentration was decreased from 500 mM to 50 mM.[62] This makes binding to the inner leaflet in our system, which has a salt concentration of 300 mM inside more unfavorable than binding to the outer leaflet where the salt concentration is 10 mM. Because this may be inhibiting translocation, it would be interesting to construct a transmembrane potential across our LUVs using the valinomycin technique to examine MPP translocation.

4.0 CONCLUSIONS AND FUTURE WORK

In conclusion, we have shown that the mitochondria-penetrating peptide with amino acid sequence Cha – Arg – Cha – Lys binds to model mitochondrial membranes in a fashion that supports the electroporation model, without disrupting the integrity of the membrane. At a low peptide-to-lipid ratio of P:L = 1:40, the MPP binds to the outer leaflet of the bilayer. At a high peptide-to-lipid ratio, P:L = 1:10, the concentration surpasses the threshold for electroporation and the peptide distributes in both the inner and outer leaflet.

However, we have not observed the MPP reaching the interior of our vesicles. To test the hypothesis that cardiolipin in the LUVs is causing limiting membrane curvature, we are going to examine the interaction of the MPP with model plasma membranes, such as LUVs composed of phosphatidylcholine and phosphatidylserine. Also, to eliminate the possibility that our salt concentration is prohibiting translocation, we are considering forming LUVs with a transmembrane gradient induced by valinomycin.

Furthermore, we would like to learn more about the forces stabilizing the MPP in the membrane – water interface to assess the depth of the energy wells in the IMM. Thus far, our work has indicated the possibility of a guanidinium – phosphate hydrogen bond because of the insertion depth of the peptide near the top of the acyl chains. ^{13}C – ^{31}P rotational echo double resonance (REDOR) experiment is an experiment that confirms the presence of this interaction.

REDOR is a powerful NMR tool that uses MAS and cross-polarization to measure the distance between two heteronuclei. Similar studies on CPPs have shown evidence of a guanidinium – phosphate hydrogen bond through this method which showed a distance of ~4 Å between the Cδ of Arg and the phosphorus of the lipid phosphate headgroup (Figure 14).[13,63-64]

In order to determine the orientational constraints of MPPs within the bilayer, we are also considering ^{15}N – ^{1}H and ^{13}C – ^{1}H dipolar chemical shift correlation experiments. If the positively charged MPP side chains are non-covalently tethered to the negatively phospholipid headgroups, the Arg and Lys side chains would have higher order parameters near the cation due to restricted mobility.[54] Consequently, the rest of the side chain and backbone would have lower order parameters and move more freely in the membrane.[54]

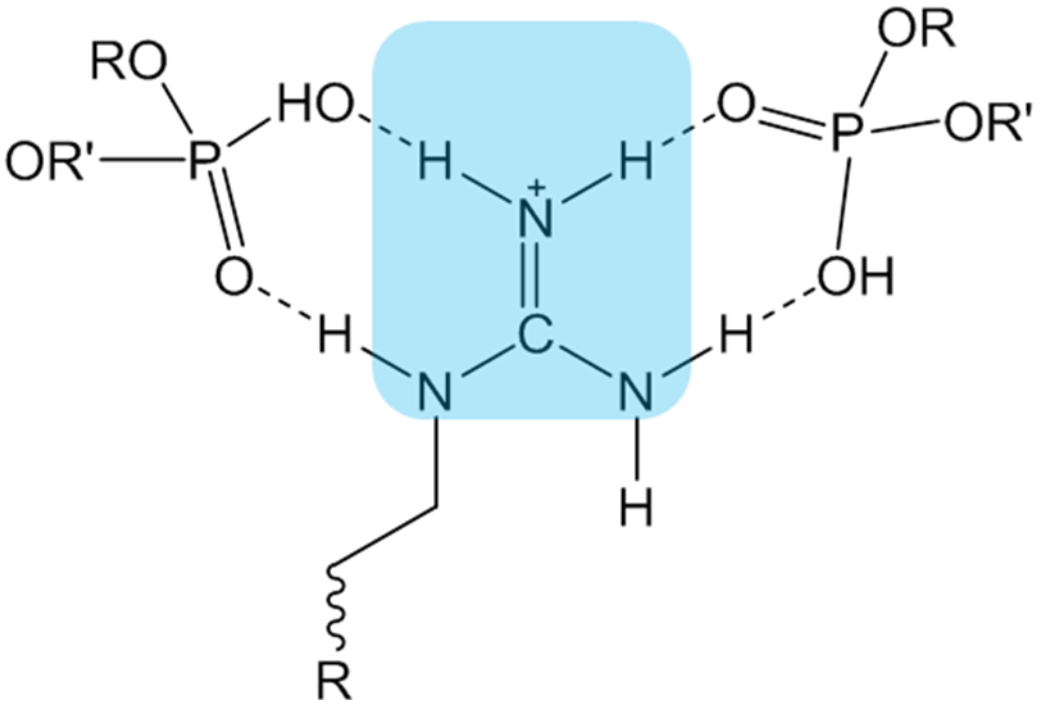

Figure 14. Image of the hydrogen bonding between the positively charged arginine side chain and the phospholipid headgroups.[66]

Additionally, open questions remain about the assembly of peptide aggregates to induce translocation. Experiments to determine exactly how much the MPPs need to interact with one another to penetrate the bilayer can provide information on aggregation. In the proposed electroporation model, the peptides must act together to cause a significant positive charge on the outer leaflet. To examine this, we are considering $^{13}C - {}^{13}C$ correlation experiments to determine if there are any aggregate structures forming amongst the peptides themselves. This experiment would be particularly interesting to perform at low peptide-to-lipid ratios to observe how the MPPs act together to build surface charge to further depolarize the membrane.

Since we believe that the MPP is proceeding via an electroporation method, we are planning to perform more experiments to assess the nature of the transient pores. For example, the pores could span the entire length of the membrane, from the inner to outer leaflet, which would cause leakage of cell contents, thus decreasing the MPP utility for drug delivery. However, it is believed that these transient pores prevent leakage in some way. Perhaps the peptide is burrowing inside of the bilayer as the membrane repairs itself simultaneously. We can assess whether or not the MPP forms pores by performing a calcein leakage assay.[65] Calcein is a fluorescent molecule, that when inside LUVs at a high enough concentration is self-quenching. If the lamellarity of the vesicles is comprised, the calcein is released and an increase in fluorescence is observed. Therefore, we can titrate a solution that has calcein encapsulated LUVs with the peptide. By using this experiment, we can determine if leakage occurs, and at what peptide concentration, based on when a fluorescence response is observed.

Lastly, this study only examined one MPP with the amino acid sequence of Cha – Arg – Cha – Lys, and the Kelley group synthesized several different peptides that were able to localize in the mitochondria.[16] As shown in Figure 14, several compounds with a +3 charge and a range

of lipophilicity were synthesized.[16] Since different cell-penetrating peptides are reported to possess vastly different mechanisms of uptake[2] it would be of interest to determine whether the same applies to mitochondria-penetrating peptides, or if one mechanism is universal. From the data presented in Figure 14, we would like to examine the mechanisms of compounds 2, 3, and 4 and see how they compare to the electroporation model proposed for compound 5.

Additionally, it has been proposed that the mechanism of internalization for cell penetrating peptides is cargo-dependent.[66-67] A variety of therapeutic agents could be delivered to mitochondria via MPPs. For example, antioxidants to capture free radicals from the electron transport chain or nucleic acids for gene modulation would be tremendously useful.[20] It would be interesting to study the different dynamics of model mitochondrial membranes if cargo is covalently attached to MPPs. Using model membranes and solid state NMR to determine the biological response of membranes would be a safe, conservative way to evaluate potential therapeutics.

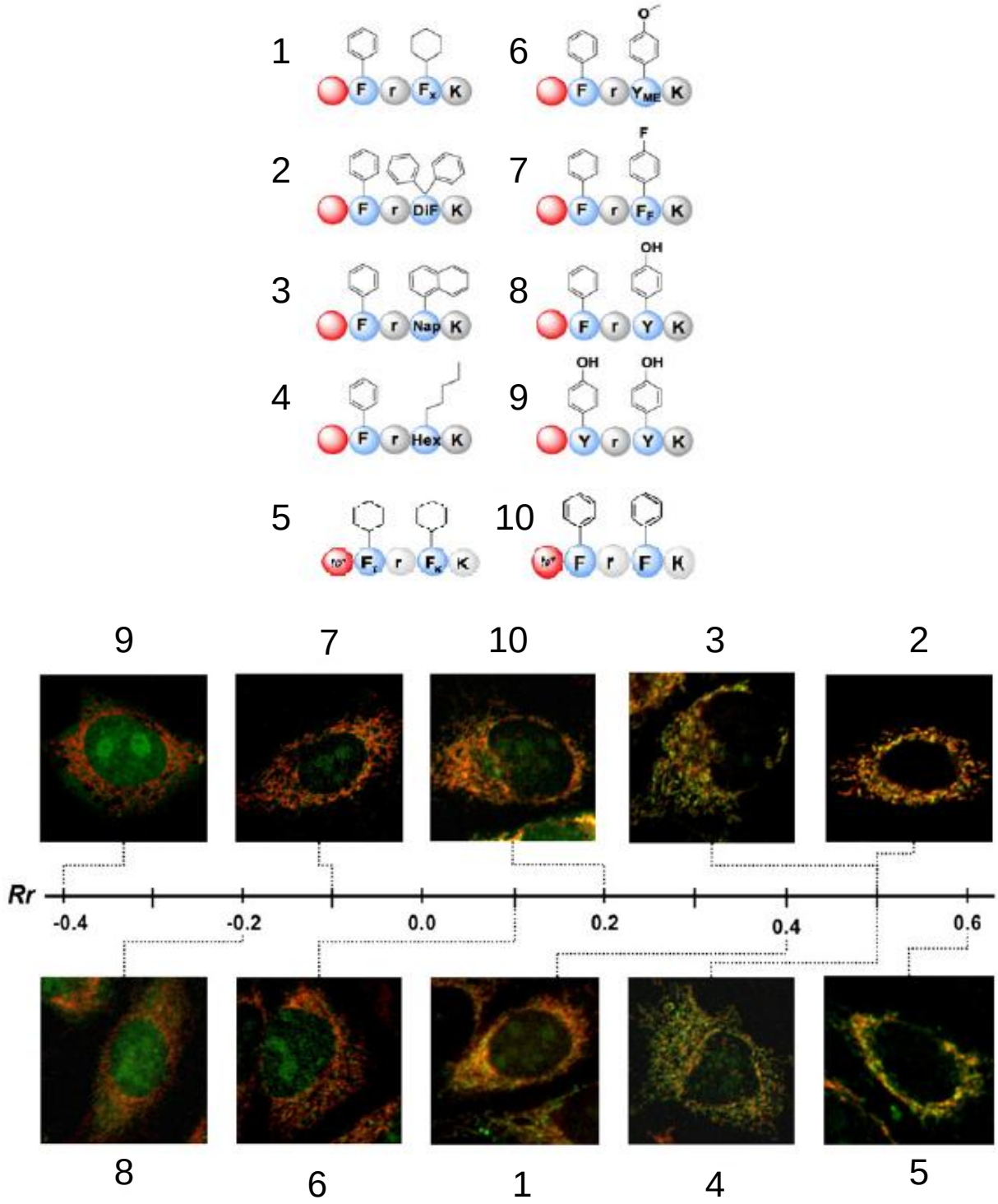

Figure 15. The +3 peptide scaffolds and the quantitation of mitochondrial localization via calculation of Rr based on fluorescence response of fluorophore linked to the peptides, *to* (thiazole orange), compared to MitoTracker. Compounds 2, 3, 4, and 5 (the MPP examined in our work) exhibit high mitochondrial localization. Image adapted from Horton et al.[18]

BIBLIOGRAPHY

(1) Deshayes, S.; Morris, M. C.; Divita, G.; Heitz, F. *Cellular and Molecular Life Sciences* **2005**, *62*, 1839.

(2) *The Handbook of Cell-Penetrating Peptides*; 2 ed.; Langel, U., Ed.; CRC Press Taylor & Francis Group: Boca Raton, FL, 2006.

(3) Hansen, M.; Kilk, K.; Langel, Ü. *Advanced Drug Delivery Reviews* **2008**, *60*, 572.

(4) Zorko, M.; Langel, Ü. *Advanced Drug Delivery Reviews* **2005**, *57*, 529.

(5) Sebbage, V. *Bioscience Horizons* **2009**, *2*, 64.

(6) Vivès, E.; Schmidt, J.; Pèlegrin, A. *Biochimica et Biophysica Acta (BBA) - Reviews on Cancer* **2008**, *1786*, 126.

(7) Binder, H.; Lindblom, G. *Biophys J* **2003**, *85*, 982.

(8) Cahill, K. *IET Systems Biology* **2010**, *4*, 367.

(9) Zhang, W.; Smith, S. O. *Biochemistry* **2005**, *44*, 10110.

(10) Derossi, D.; Chassaing, G.; Prochiantz, A. *Trends in Cell Biol.* **1998**, *8*, 84.

(11) Derossi, D.; Joliot, A. H.; Chassaing, G.; Prochiantz, A. *Journal of Biological Chemistry* **1994**, *269*, 10444.

(12) Prochiantz, A. *Current Opinion in Neurobiology* **1996**, *6*, 629.

(13) Su, Y.; Mani, R.; Hong, M. *J Am Chem Soc* **2008**, *130*, 8856.

(14) Fantin, V. R.; Leder, P. *Oncogene* **0000**, *25*, 4787.

(15) Galluzzi, L.; Larochette, N.; Zamzami, N.; Kroemer, G. *Oncogene* **0000**, *25*, 4812.

(16) Horton, K. L.; Stewart, K. M.; Fonseca, S. B.; Guo, Q.; Kelley, S. O. *Chemistry & Biology* **2008**, *15*, 375.

(17) Murphy, M. P.; Smith, R. A. J. *Advanced Drug Delivery Reviews* **2000**, *41*, 235.

(18) Scheffler, I. E.; 2 ed.; John Wiley & Sons, Inc.: Hoboken, New Jersey, 2008.

(19) Yousif, L. F.; Stewart, K. M.; Horton, K. L.; Kelley, S. O. *Chembiochem* **2009**, *10*, 2081.

(20) Yousif, L. F.; Stewart, K. M.; Kelley, S. O. *Chembiochem* **2009**, *10*, 1939.

(21) Bradham, C. A.; Qian, T.; Streetz, K.; Trautwein, C.; Brenner, D. A.; Lemasters, J. J. *Mol. Cell. Biol.* **1998**, *18*, 6353.

(22) Goossens, V.; Grooten, J.; De Vos, K.; Fiers, W. *Proceedings of the National Academy of Sciences of the United States of America* **1995**, *92*, 8115.

(23) Brand, M. D. *Biochimica et Biophysica Acta (BBA) - Bioenergetics* **1990**, *1018*, 128.

(24) Hafner, R. P.; Leake, M. J.; Brand, M. D. *FEBS Letters* **1989**, *248*, 175.

(25) Paradies, G.; Petrosillo, G.; Ruggiero, F. M. *Biochimica et Biophysica Acta (BBA) - Bioenergetics* **1997**, *1319*, 5.

(26) Corral-Debrinski, M.; Shoffner, J. M.; Lott, M. T.; Wallace, D. C. *Mutation Research/DNAging* **1992**, *275*, 169.
(27) Ferrari, R. *Journal of Cardiovascular Pharmacology* **1996**, *28*, 1.
(28) Lesnefsky, E. J.; Moghaddas, S.; Tandler, B.; Kerner, J.; Hoppel, C. L. *Journal of Molecular and Cellular Cardiology* **2001**, *33*, 1065.
(29) Pavlakis, S. G.; Phillips, P. C.; DiMauro, S.; De Vivo, D. C.; Rowland, L. P. *Annals of Neurology* **1984**, *16*, 481.
(30) Sessa, G.; Weissmann, G. *Journal of Lipid Research* **1968**, *9*, 310.
(31) Tamm, L. K.; McConnell, H. M. *Biophys J* **1985**, *47*, 105.
(32) Bangham, A. D.; Standish, M. M.; Watkins, J. C. *Journal of Molecular Biology* **1965**, *13*, 238.
(33) Moscho, A.; Orwar, O.; Chiu, D. T.; Modi, B. P.; Zare, R. N. *Proceedings of the National Academy of Sciences of the United States of America* **1996**, *93*, 11443.
(34) Deamer, D.; Bangham, A. D. *Biochimica et Biophysica Acta (BBA) - Nucleic Acids and Protein Synthesis* **1976**, *443*, 629.
(35) Huang, C.-H. *Biochemistry* **1969**, *8*, 344.
(36) Hope, M. J.; Bally, M. B.; Mayer, L. D.; Janoff, A. S.; Cullis, P. R. *Chemistry and Physics of Lipids*, *40*, 89.
(37) Hong, M. *Structure* **2006**, *14*, 1731.
(38) *Spin dynamics: basics of nuclear magnetic resonance*; 2 ed.; Levitt, M. H., Ed.; John Wiley & Sons, 2008.
(39) Zandomeneghi, G., 2003.
(40) Mason, J. *Solid State Nucl Magn Reson* **1993**, *2*, 285.
(41) Duer, M. J. *Introduction to Solid State NMR Spectroscopy*; Blackwell Publishing Ltd: Oxford, UK, 2004.
(42) Dopico, A. *Methods in membrane lipids*; Humana, 2007.
(43) Andrew, E. R.; Bradbury, A.; Eades, R. G. *Nature* **1959**, *183*, 1802.
(44) Lowe, I. J. *Physical Review Letters* **1959**, *2*, 285.
(45) Buffy, J. J.; Hong, T.; Yamaguchi, S.; Waring, A. J.; Lehrer, R. I.; Hong, M. *Biophys J* **2003**, *85*, 2363.
(46) Nolden, P. W.; Ackermann, T. *Biophysical Chemistry* **1976**, *4*, 297.
(47) Cullis, P. R.; Bally, M. B.; Madden, T. D.; Mayer, L. D.; Hope, M. J. *Trends in Biotechnology* **1991**, *9*, 268.
(48) Casadio, R.; Baccarini-Melandri, A.; Melandri, B. A. *European Journal of Biochemistry* **1974**, *47*, 121.
(49) Lewis, R. N. A. H.; Zweytick, D.; Pabst, G.; Lohner, K.; McElhaney, R. N. *Biophys J* **2007**, *92*, 3166.
(50) Kupiainen, M.; Flack, E.; Ollila, S.; Niemella, P.; Gurtovenko, A. A.; Hyvonen, M. T.; Patra, M.; Karttunen, M.; Vattulainen, I. *Journal of Computational and Theoretical Nanoscience* **2005**, *2*, 401.
(51) Seddon, J. M.; Cevc, G.; Kaye, R. D.; Marsh, D. *Biochemistry* **1984**, *23*, 2634.
(52) Hristova, K.; White, S. H. *Biochemistry* **2005**, *44*, 12614.
(53) Wimley, W.; White, S. *Nature Structural & Molecular Biology* **1996**, *3*, 842.
(54) Su, Y.; Waring, A. J.; Ruchala, P.; Hong, M. *Biochemistry* **2010**, *49*, 6009.
(55) White, S. H.; Wimley, W. C. *Annual Review of Biophysics and Biomolecular Structure* **1999**, *28*, 319.

(56) Wimley, W. C.; Creamer, T. P.; White, S. H. *Biochemistry* **1996**, *35*, 5109.
(57) Rothbard, J. B.; Jessop, T. C.; Lewis, R. S.; Murray, B. A.; Wender, P. A. *J Am Chem Soc* **2004**, *126*, 9506.
(58) Persson, D.; Thorén, P. E. G.; Esbjörner, E. K.; Goksör, M.; Lincoln, P.; Nordén, B. *Biochimica et Biophysica Acta (BBA) - Biomembranes* **2004**, *1665*, 142.
(59) Terrone, D.; Sang, S. L. W.; Roudaia, L.; Silvius, J. R. *Biochemistry* **2003**, *42*, 13787.
(60) Khalifat, N.; Puff, N.; Bonneau, S.; Fournier, J.-B.; Angelova, M. I. *Biophys J* **2008**, *95*, 4924.
(61) Tom i , N. Babnik, B. Lombardo, D. Mav i , B. a ndu er, M. Igli , A. r alj-Igli , V. *Journal of Chemical Information and Modeling* **2005**, *45*, 1676.
(62) Ben-Tal, N.; Honig, B.; Peitzsch, R. M.; Denisov, G.; McLaughlin, S. *Biophys J* **1996**, *71*, 561.
(63) Su, Y.; Doherty, T.; Waring, A. J.; Ruchala, P.; Hong, M. *Biochemistry* **2009**, *48*, 4587.
(64) Tang, M.; Waring, A. J.; Hong, M. *J Am Chem Soc* **2007**, *129*, 11438.
(65) Schwarz, G.; Arbuzova, A. *Biochimica et Biophysica Acta (BBA) - Biomembranes* **1995**, *1239*, 51.
(66) Alves, I. D.; Correia, I.; Jiao, C. Y.; Sachon, E.; Sagan, S.; Lavielle, S.; Tollin, G.; Chassaing, G. *Journal of Peptide Science* **2009**, *15*, 200.
(67) Elsa, B.-W.; Jugnu, G.; Pontus, L.; Ülo, L.; Astrid, G. *FEBS Letters* **2007**, *581*, 2389.